PCCP

RSC Publishing

PAPER

Understanding the effect of side groups in ionic liquids on carbon-capture properties: a combined experimental and theoretical effort†

Cite this: *Phys. Chem. Chem. Phys.*, 2013, **15**, 3264

Fangyong Yan,[ab] Michael Lartey,[c] Krishnan Damodaran,[cd] Erik Albenze,[ce] Robert L. Thompson,[ce] Jihan Kim,[b] Maciej Haranczyk,[g] Hunaid B. Nulwala,*[cf] David R. Luebke*[c] and Berend Smit*[ab]

Ionic liquids are an emerging class of materials with applications in a variety of fields. Steady progress has been made in the creation of ionic liquids tailored to specific applications. However, the understanding of the underlying structure–property relationships has been slower to develop. As a step in the effort to alleviate this deficiency, the influence of side groups on ionic liquid properties has been studied through an integrated approach utilizing synthesis, experimental determination of properties, and simulation techniques. To achieve this goal, a classical force field in the framework of OPLS/Amber force fields has been developed to predict ionic liquid properties accurately. Cu(I)-catalyzed click chemistry was employed to synthesize triazolium-based ionic liquids with diverse side groups. Values of densities were predicted within 3% of experimental values, whereas self-diffusion coefficients were underestimated by about an order of magnitude though the trends were in excellent agreement, the activation energy calculated in simulation correlates well with experimental values. The predicted Henry coefficient for CO_2 solubility reproduced the experimentally observed trends. This study highlights the importance of integrating experimental and computational approaches in property prediction and materials development, which is not only useful in the development of ionic liquids for CO_2 capture but has application in many technological fields.

Received 5th November 2012,
Accepted 8th January 2013

DOI: 10.1039/c3cp43923b

www.rsc.org/pccp

1. Introduction

An important field of research is finding novel materials to efficiently capture carbon. Different materials and processes have been proposed to increase the efficiency of the separation of CO_2.[1,2] A promising class of materials are supported ionic liquid membranes.[3–5] A unique property of these ionic liquids is that a very large number of possible materials[6] can be synthesized, which gives us a route to tailor make an ionic liquid with exactly the right material properties.[7–10] Molecular simulation can be a useful tool to obtain better insights into the relation between the molecular structure and properties of these ionic liquids.[11–17]

Few systematic studies have been carried out examining whether computational studies can accurately predict the properties of ionic materials. Most theoretical studies rely on experimental data, which are seldom available for exactly the system of theoretical interest. Similarly, theoretical predictions can only be tested experimentally if the materials can be synthesized. Synthetic chemistry and theoretical modeling need to be conducted in tandem to accurately predict properties and develop structure–property relationships.

Imidazolium-based ionic liquids have been the focus of much research with major emphasis on aliphatic side groups.[12,13,18–20] In this work, we take advantage of a related class of ionic liquids that were prepared using click chemistry, as shown in Fig. 1.

[a] *Department of Chemical and Biomolecular Engineering, University of California, Berkeley, 201 Gilman Hall, Berkeley, CA 94720, USA. E-mail: Berend-Smit@Berkeley.edu; Fax: +1-(510) 642-4778; Tel: +1-(510) 642-4778*

[b] *Materials Sciences Division, Lawrence Berkeley National Laboratory, Berkeley, CA 94720, USA*

[c] *National Energy Technology Laboratory, P.O. Box 10940, Pittsburgh, PA 15236, USA. E-mail: david.luebke@netl.doe.gov; Fax: +1-(412) 386-4604; Tel: +1-(412) 386-4118*

[d] *Department of Chemistry, University of Pittsburgh, Pittsburgh, PA 15260, USA*

[e] *URS Corporation, P.O. Box 618, South Park, Pennsylvania 15219, USA*

[f] *Department of Chemistry, Carnegie Mellon University, 4400 Fifth Avenue, Pittsburgh, Pennsylvania 15213, USA. E-mail: hnulwala@andrew.cmu.edu; Fax: +1-(412) 929-8102; Tel: +1-(412) 268-5927*

[g] *Computational Research Division, Lawrence Berkeley National Laboratory, Berkeley, CA 94720, USA*

† Electronic supplementary information (ESI) available. See DOI: 10.1039/c3cp43923b

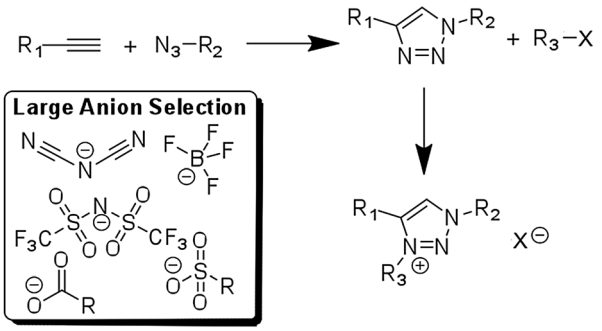

Fig. 1 The modular nature of ionic liquids allows us to synthesize a large number of structures utilizing click chemistry.

The Cu(I) catalyzed azide–alkyne cycloaddition allows a series of ionic liquids to be quickly synthesized with absolute control over chemical structure.[21] The main advantages of the click reaction are regio-specificity and the ability to construct molecules with many possible side-groups.

Herein, click chemistry and molecular simulation have been used in tandem to enable a systematic approach for developing structure–property relationships. Additionally, this tandem approach has high confidence as it alleviates the problems associated with finding the data from the literature to verify the results.

The new force fields are based on the triazolium core. A number of functional groups were evaluated and verified with experimental data. To the best of our knowledge, this is the first experimentally verified molecular simulation study on 1,2,3-triazolium-based ionic liquids with different polar and non-polar side groups. These groups include aliphatic, aromatic, ethereal and silane-based side groups. The insight gained from this study on the effects of side groups is valuable and transposable onto other families of ionic liquids.

2. Experimental details

IL synthesis and characterization methods: All chemicals were purchased with the highest purity from commercial sources and used as received. ^{1}H (300 to 700 MHz), ^{13}C (75 to 176 MHz) and ^{19}F (471 to 565 MHz) NMR spectra were recorded in $CDCl_3$ or DMSO-d_6 on a Bruker Avance III 500 or 700 spectrometer. The density of the ionic liquids was determined using an automatic density meter (Model DDM 2911 from Rudolph Research Analytical) or a gas pycnometer (AccuPyc II 1390 from Micromeritics) at room temperature. For detailed chemical characterization see ref. 21 and Section S2 (ESI†).

All solubility measurements were performed using a PCT-Pro 2000 apparatus from Setaram Inc. The PCT-Pro 2000 is a Sievert's apparatus, which determines gas solubility in a sample by charging a leak-tight sample chamber of known volume with a known quantity of CO_2. The CO_2-charged sample chamber is isolated from the rest of the system and the pressure drop in the chamber is measured. The drop in pressure due to CO_2 absorption into the liquid is then measured, and the quantity of CO_2 absorbed into the liquid is easily determined from an equation of state, in this case, the NIST Standard Reference Database 23.[22,23] For all tests, between 0.9 g and 1.5 g of the sample was loaded into the sample chamber. The sample was held under a dynamic vacuum for 4 hours prior to starting a test. During this evacuation, the sample was heated to 30 °C and was stirred at 300 rpm. After evacuation, testing was initiated by dosing the sample chamber with a known amount of CO_2, and the sample was allowed to equilibrate for at least 4 hours. Dosing was repeated to obtain an isotherm over a pressure range of 0–10 bar. Throughout all tests, the sample was held at 30 °C and was stirred at 300 rpm.

Self-diffusion coefficient measurements were performed using a Bruker Avance III 600 MHz spectrometer with a BBFO probe with the *Z*-axis gradient. Temperatures were controlled to ±1 K accuracy using a Bruker BVT3000 temperature control system. The samples were thermally equilibrated at each temperature for 30 min before the measurements. All the experiments were performed on neat samples without any deuterated solvents. Extensive shimming was done on each sample prior to acquisition to observe JHH splitting. The measurements of the self-diffusion coefficients for the cation and the anion in each ionic liquid were made by using ^{1}H and ^{19}F nuclei, respectively. Self-diffusion coefficients were determined using a Stimulated Echo Pulsed Field Gradient (STE-PFG) pulse sequence with bipolar gradients.[24,25] To obtain the self-diffusion coefficient, the peak intensity *vs.* gradient strength data were fit to the Stejskal–Tanner equation.[26,27]

$$\frac{I}{I_0} = \exp\left[-\gamma^2 g^2 \delta^2 \left(\Delta - \tfrac{\delta}{3}\right) D_s\right] \quad (1)$$

where I and I_0 are the signal intensities with and without gradients, respectively, γ is the gyromagnetic ratio, g is the gradient strength, δ is the length of the gradient pulses, Δ is the diffusion time between the gradient pulses, and D_s is the self-diffusion coefficient. The gradient strength was varied between 0 and 50 G cm^{-1}, while the duration of the gradient δ was held constant throughout the experiment. δ was set between 2 and 5 ms while the diffusion time Δ was kept constant at 300 ms depending on the diffusion rate of different samples and at different temperatures.

3. Computation details

Fig. 2 shows the class of ionic liquids we study in this work. To describe the interactions between the atoms, we constructed a force field following the methodology of Lopes *et al.*[28,29] This force field takes the form:

$$\begin{aligned} U_{\text{total}} = & \sum_{ij}^{\text{bonds}} \frac{K_{r,ij}}{2}\left(r_{ij} - r_{0,ij}\right)^2 + \sum_{ijk}^{\text{angles}} \frac{k_{\theta,ijk}}{2}\left(\theta_{ijk} - \theta_{0,ijk}\right)^2 \\ & + \sum_{ijkl}^{\text{dihedrals}} \sum_{m=1}^{4} \frac{V_{m,ijkl}}{2}\left[1 + (-1)^m \cos\left(m\phi_{ijkl}\right)\right] \\ & + \sum_{i} \sum_{j \neq i} \left\{ 4\varepsilon_{ij}\left[\left(\frac{\sigma_{ij}}{r_{ij}}\right)^{12} - \left(\frac{\sigma_{ij}}{r_{ij}}\right)^{6}\right] + \frac{q_i q_j}{r_{ij}} \right\} \end{aligned} \quad (2)$$

where $K_{r,ij}$, $k_{\theta,ijk}$, and $V_{m,ijkl}$ are force constants for bond stretching, bond angle bending, and dihedral angle motion, respectively; r_{ij}, θ_{ijk}, and $\theta_{0,ijk}$ are instantaneous bond length, bond angle and dihedral angle, respectively; $r_{0,ij}$ and $\theta_{0,ijk}$ are

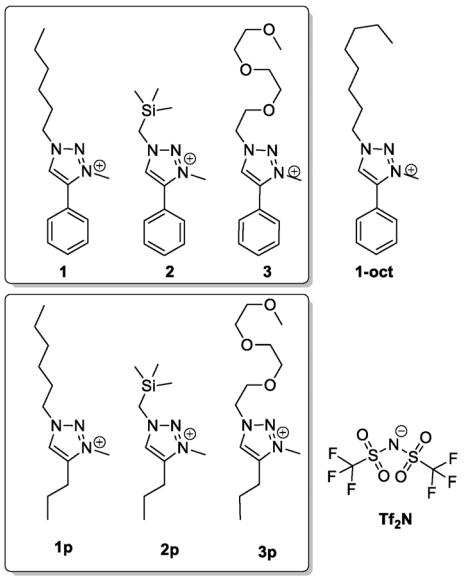

Fig. 2 Chemical structures of ionic liquids evaluated in this study. All triazolium-based ionic liquids contain the same anion, bis[(trifluoromethyl)-sulfonyl]imide (Tf_2N), and the triazolium ring bears three substituent groups, R_1, R_2, and R_3. R_3 has been kept constant as a methyl group in this study. The ionic liquids are in two groups, when R_1 is a phenyl group, the ionic liquid is named as n, such as hexyl (1), (trimethylsilyl)methylene (TMS) (2), and tri-(ethylene glycol) methyl ether, $CH_3(OCH_2CH_2)_3$ (3). When R_1 is a propyl group, the ionic liquid is named as np, where n follows the same terminology. The only exception in this naming is 1-oct.

equilibrium bond length, bond angle, respectively; and m is the multiplicity for the dihedral angle. The nonbonded energy terms are represented by Coulomb and Lennard-Jones (LJ) potentials, where ε_{ij} and σ_{ij} are LJ parameters, and q_i is the point partial charge.

All *ab initio* calculations used the Gaussian 09 package.[30] We obtained the equilibrium geometry ($r_{0,ij}$,$\theta_{0,ijk}$) using optimization at the level of RHF/6-31 G(d). We obtained the partial charges q_i using the CHelpG[31] method at the level of MP2/cc-pVTZ(-f)//RHF/6-31G(d) for obtaining the electron densities. All charges are shown in Fig. S3-1 (ESI†). We obtained the bond force constant $K_{r,ij}$ and bond angle force constant $k_{\theta,ijk}$, from AMBER[32] and OPLS[33] force fields. Unknown force constants were calculated based on empirical formulas from the general Amber force field (Gaff).[34] We obtained the dihedral angle force constant $V_{m,ijkl}$ by fitting the molecular mechanics simulation to the *ab initio* calculations. We first ran the dihedral angle potential scan at the level of HF/6-31G(d). The scan spans from 0.0 to 180.0, with 100 for each step. After we obtained the geometries for each step, we used MP2/cc-PVTZ(-f) to calculate the single-point potential energy. An example of the dihedral angle potential scan for the dihedral angle between the phenyl group and the core of ionic liquid 2, and the dihedral angle potential fitting, which shows a perfect match, is shown in Fig. S3-2 (ESI†). All force constants can be found in Tables S3-1–S3-5 (ESI†).

The density and self-diffusion coefficients were determined using molecular dynamics (MD) simulations. All MD simulations are conducted using a parallel version of Gromacs 4.5.4.[35] During the simulation a fully relaxed model and a time step of 1.5 fs were used. The long range electrostatic interactions were treated with the smooth particle mesh Ewald (SPME)[36] method with a PME of 4th order and an Ewald convergence of 10×10^{-6}. A cut-off distance of 1.2 nm was used for both short-range van der Waals interactions and real-space electrostatic interactions. All simulations were conducted in the isothermal–isobaric ensemble (NPT) at 1 atmosphere using a Nose–Hoover[37,38] thermostat and an isotropic Parrinello–Rahman barostat[39] with relaxation times of 1 and 5 ps, respectively.

Simulation employed system sizes of 500 pairs for all ionic liquids. This size is among the largest atomistic simulations of ionic liquids, and it is used to minimize the finite-size effects. All simulations started in cubic boxes with densities as low as 0.001 g cm^{-3}. The systems were subsequently compressed to a high pressure (10 000 bar at 50 K) until the systems reached a density close to 1.0 g cm^{-3}. The systems were then heated up to 600 K over 2–3 ns at 1 atm confirming that the systems were isotropic and at equilibrium. Following this treatment, all systems were cooled to the target temperatures using a simulated annealing procedure. All simulation systems run at a time scale of 30–50 ns.

4. Results and discussion

The simulation and experimental densities of all ionic liquids are shown in Fig. 3. The predicted density is close to the experimental density (difference is less that 3%), but systematically over predicts the density. More importantly, Fig. 3a shows that for the same substitution group R_1, the density increases as the order of

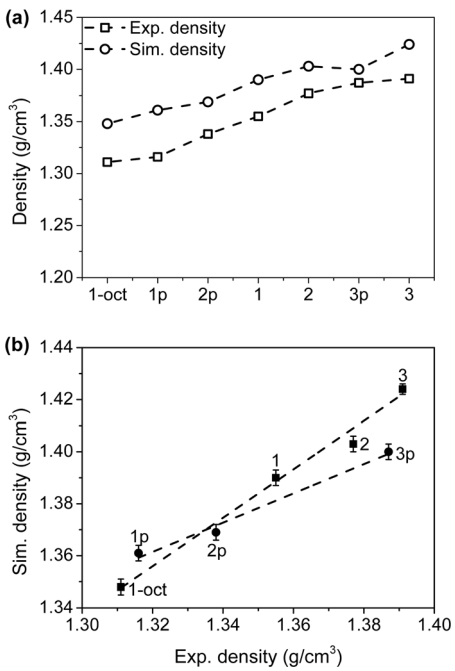

Fig. 3 (a) Density of ionic liquids 1-oct, 1p, 2p, 1, 2, 3p, 3 in both simulation and experiment at 298 K, all data are listed in Table S1-1 (ESI†). (b) Linear correlation for experiment and simulated density of 1-oct, 1, 2, and 3, and 1p, 2p and 3p.

substitution oxyl group > silane group > aliphatic group. For the same substitution group at R_2, n > np, the phenyl group leads to higher density than the propyl group. Fig. 3b shows these two trends more clearly by using the density correlation plot between experiment and simulation. A linear but different correlation is found for n and np, where the slope of n is higher than np, indicating that the phenyl group has a higher density trend than the propyl group. This linear correlation also shows that our force field correctly captures the microscopic individual cations structure changes underlying the macroscopic behaviour of these ionic liquids.

To characterize the structure of the ionic liquids the radial distribution function (RDF) was calculated (illustrated in Fig. 4a at 373 K), where four different types are characterized: center of mass of triazolium core–anion, center of mass of cation–anion, center of mass of cation–cation, and center of mass of anion–anion.

The cation–anion RDF shows a peak, which indicates that the cation and the anion form coordinated regions due to the strong coulombic interaction. The anion–anion and cation–cation show no peak suggesting that the cations are distributed randomly relative to cations, and that the anions are also distributed randomly relative to others anions, due to the coulomb repulsion. The RDF for the triazolium core and anions shows that the core–anion interaction has a higher intensity than cation–anion, which is due to the fact that +1 charge is located mainly around the triazolium core (see Fig. S3-1, ESI†). We also compared the center of mass of cation–anion radial distribution functions for different ionic liquids in Fig. 4b. We found that ionic liquid n has higher intensity than the corresponding np, which shows that the cation and the anion in n pack together more closely than np, causing the higher density in n than in np. When the set (3p, 3) is compared to (1, 1p, 1-oct) and (2, 2p) it is observed that it has more liquid-like structure. This property may be due to the fact that the oxyl group in 3 and 3p is polar and can interact with the anion and weaken the interactions between the triazolium-core and the anion. For 1 (1p) and 2 (2p), the cation–anion distribution is more structured in 2 than in 1. This result follows the density trend. The most structured cation–anion RDF is for 1-oct despite the lowest density among all ionic liquids. In order to understand this phenomenon, tail–atom RDFs were calculated for 1 and 1-oct as illustrated in Fig. 4c, where tail–atom is the end of the carbon atom of hexyl or octyl, respectively. It was found that in the case of 1-oct tail–tail interaction is stronger in the case of octyl than the hexyl group. This indicates that octyl species pack strongly together and form non-polar domains. This microphase domain separation creates more free volume, and results in a lower density. This non-polar domain formed by aliphatic chains has also been found in imidazolium-based ionic liquids as reported by Wang and Voth,[40] who noted that when the substitution groups are aliphatic chains and the carbon number exceeds 4, the aliphatic chains tend to aggregate together to form domains and also result in lower densities.

We have also examined the self-diffusion coefficients of the cations and anions. The self-diffusion coefficient is an important

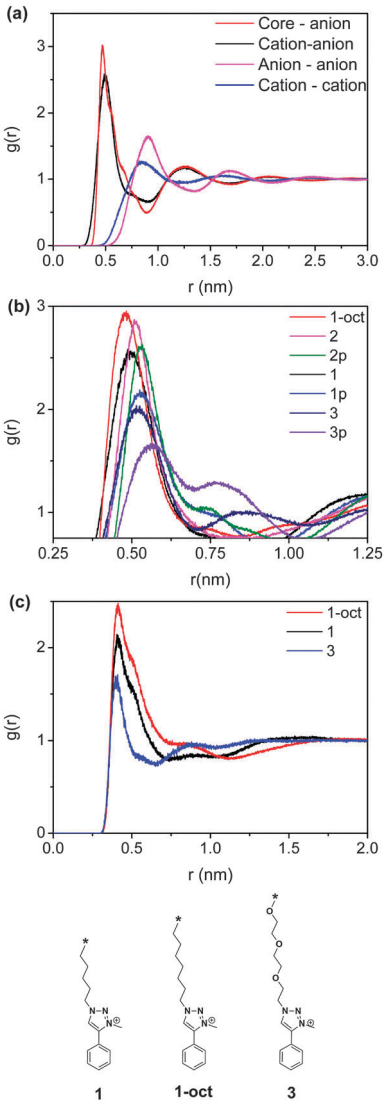

Fig. 4 (a) Radial distribution function of ionic liquid 1 at 373 K. (b) Radial distribution function of cation–anion of 1-oct, 1, 2, 3, 1p, 2p, and 3p at 373 K. (c) Radial distribution function of tail–tail carbon atom of 1, 1-oct, and 3. The tail atom is defined as the end carbon atom (*) of the functional group of 1, 1-oct and 3.

dynamic property of ionic liquids. The self-diffusion coefficient D_S was calculated based on the Einstein relationship,

$$D_S = \lim_{t\to\infty} \left\langle \left| \overrightarrow{r(t)} - \overrightarrow{r(0)} \right|^2 \right\rangle \quad (3)$$

where t is the time, and $\left| \overrightarrow{r(t)} - \overrightarrow{r(0)} \right|^2$ is the mean square displacement (MSD).

Fig. 5a shows the mean-squared displacement (MSD) of the cation and the anion of ionic liquid 1p at 480 K. Due to the slow dynamics of ionic liquids,[41] it is necessary to check whether the cation–anion system has reached the true diffusive regime. To check this, ln(MSD/t) *versus* ln(t) was calculated. The true diffusive regime has been reached when the curve reaches a plateau as illustrated in Fig. 5b for 1p at 480 K. At low

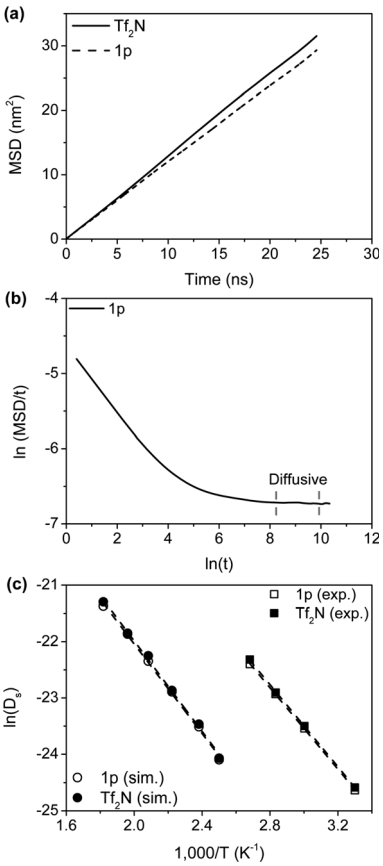

Fig. 5 (a) MSD (mean-square-displacement) of cation and anion of ionic liquid 1p. (b) Logarithm of the diffusion coefficient of cation (1p) changing with time. (c) Arrhenius relationship of ionic liquid 1p of cation and anion activation energy *versus* temperature in both experiment and simulation. Throughout this figure and caption, the designation '1p' is used to refer to the cation only while throughout the rest of the paper, '1p' is used to identify the whole IL.

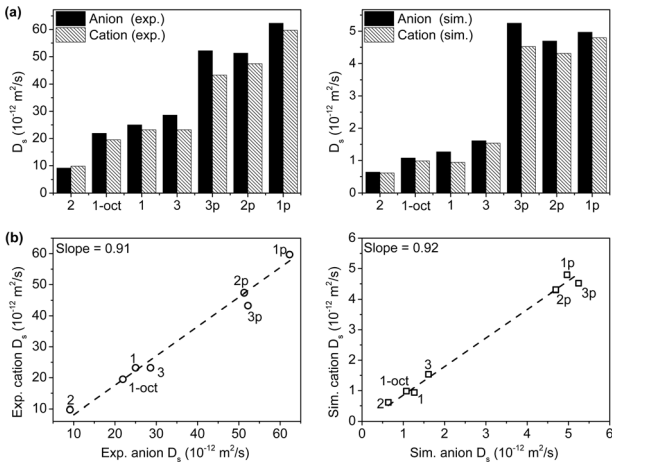

Fig. 6 (a) Experiment and simulation self-diffusion coefficient of cations and anions of all ionic liquids at 333 K. All data are listed in Tables S1-2 and S1-3 (ESI†). (b) Self-diffusion coefficient correlation of experimental cations and anions, and simulation cation and anions.

temperature, the time needed for reaching the diffusive region can exceed the computational limit of 100 ns. In order to calculate the self-diffusion coefficient at low temperature the simple Arrhenius relationship was used:

$$\ln(D_S) = -\frac{E_a}{R \times T} + \ln(D_0) \quad (4)$$

where E_a is the activation energy, R is the gas constant, T is the temperature, D_0 is the frequency factor. Fig. 5c shows an example of the Arrhenius relationship of 1p in experiment and simulation. The linear relationship in both experiment and simulation demonstrates the validity of using this method.

Self-diffusion coefficients of the cations and anions of all ionic liquids at 333 K were calculated using the Arrhenius equation. These results were compared to the experimental data and it was found that experimental diffusion coefficients were about 10 times greater than the simulated results, as shown in Fig. 6a. However, both experiment and simulation show that ionic liquid n has a lower diffusion coefficient than the corresponding liquid np. For different ionic liquids, the simulation predicts the correct order, 3 > 1 > 1-oct > 2. Ionic liquid 2 has the lowest D_S, perhaps due to its bulky non-polar (trimethylsilyl)methylene (TMS) group. Ionic liquid 3 has the weakest cation–anion interaction, and the radial distribution function of the tail atom of 3 (Fig. 4c) shows that the oxyl group does not aggregate. This result shows that 3 is the most liquid-like compared to 1 and 1-oct and should have the highest diffusion coefficient. For 1-oct and 1, because of the tail aggregation effect (Fig. 4c), 1-oct has the lower diffusion coefficient. For the case of np, the experiment shows that the order is 1p > 2p > 3p; however, the simulation predicts the order 3p > 1p > 2p. This inconsistency may be caused by the under-estimation of the density of 3p (error 0.9%) compared to other ionic liquids (error ~2–3%), as shown in Fig. 2a. In Fig. 6b, both simulation and experiment show that the cation and anion D_S are linearly correlated. The anion has a greater diffusion coefficient, which reflects its smaller size. A similar correlation slope also shows the accuracy of our force field to distinguish different cations.

Fig. 7a shows the activation energy of cations and anions of different ionic liquids in both experiment and simulation. It shows that the activation energy of np is lower than that of n giving insight into the higher diffusion coefficient of n. Fig. 7b also shows that the experimental and simulated anion (and cation) activation energy is linearly correlated, and interestingly, two types of correlations are found, one for 1, 1-oct, 1p, 2 and 2p, and another for 3 and 3p. This phenomenon can be attributed to the fact that 3 and 3p have polar substituent groups, while the other ionic liquids have non-polar substituent groups.

After validation of the force field by density quantitatively and self-diffusivity qualitatively, it was used to study CO_2 solubility using the EPM2 force field.[42] The Widom test particle insertion method[43,44] was used to calculate the Henry's Law coefficient, K_H of CO_2 in ionic liquids,

$$K_H = \rho RT \exp(\beta \mu_{ex}) \quad (5)$$

where ρ is the number density, which is defined as the number of ionic liquid pairs divided by the ionic liquid volume, β is the

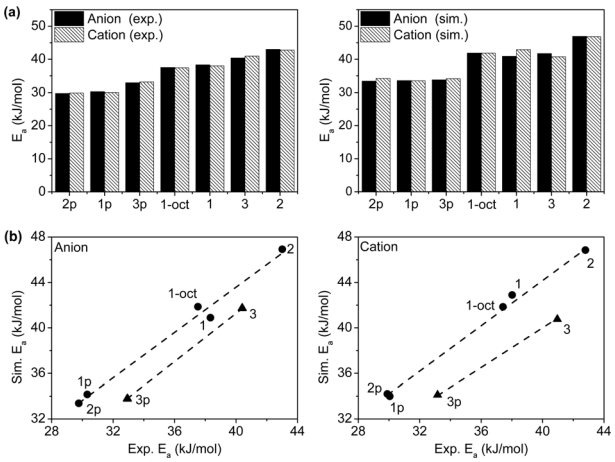

Fig. 7 (a) Experimental and simulated self-diffusion activation energy of all ionic liquids, all data are listed in Table S1-4 (ESI†). (b) Activation energy correlation of simulated and experimental anions and cations. Different correlations are observed for the polar (3, 3p) and nonpolar (1, 1-oct, 1p, 2 and 2p) substitution groups.

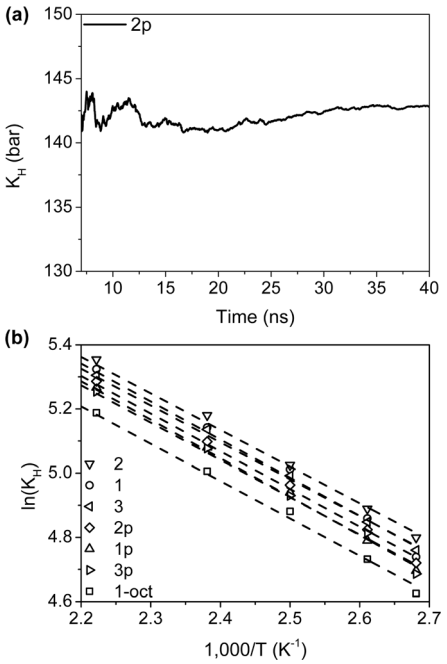

Fig. 8 (a) Henry's Law coefficient K_H calculation for ionic liquid 2p at 400 K by Widom particle insertion. (b) Logarithm of K_H of different ionic liquids as a function of temperature at 1 bar. The lines represent linear fits and are intended as a guide to the eye.

inverse temperature, μ_{ex} is the excess chemical potential of CO_2 and defined as

$$\mu_{ex} = -kT \times \ln\left(\frac{\langle V \times \exp(-\beta U_{ins})\rangle_{NPT}}{\langle V\rangle_{NPT}}\right) \quad (6)$$

where $\langle\ \rangle_{NPT}$ represents the ensemble average, V is the volume of ionic liquid, U_{ins} is the insertion potential energy of CO_2, which is defined as the interaction energy between CO_2 and ionic liquid.

An example of Widom test particle insertion is shown in Fig. 8a, where 1 million insertions per configuration are used for a total simulation time of 42 ns, and each configuration is stored every 1.5 ps. Runs of 6 ns were done for equilibrium, and 36 ns for production. Overall there were 24 billion insertions were performed. The efficiency of Widom particle insertion of CO_2 in the ionic liquid depends on the temperature. At low temperatures ionic liquids are vitrified and longer simulation times are required. For example, ionic liquid 1 at 298 K has the self-diffusion coefficient value of 3.1×10^{-13} m^2 s^{-1} and 2.4×10^{-13} m^2 s^{-1}, for anion and cation, respectively. Based on eqn (3), the mean displacements of cation and anion, $\left|\overrightarrow{r(t)} - \overrightarrow{r(0)}\right|$, for the simulation time of 100 ns, are less than 0.6 Å, which indicates that the ionic liquids are almost ''frozen''. In order to solve the problem caused by slow dynamics at low temperatures, higher temperatures are needed so that the K_H will converge. Thus, the Arrhenius equation,

$$\Delta H = R\left(\frac{\partial \ln(K_H)}{\partial(1/T)}\right)_P \quad (7)$$

where ΔH is the CO_2 heat of adsorption in the ionic liquid and the subscript ''P'' indicates constant pressure, is used to solve the Henry's Law coefficient at elevated temperatures. Fig. 8a shows such an example, where the temperature is 400 K.

Fig. 8b shows the Henry coefficient of CO_2 in all the ionic liquids at different temperatures as low as 383 K. The order of the Henry's Law coefficients is: 2 > 1 > 3 > 2p > 1p > 3p > 1-oct. Based on the Henry's law relationship,

$$P = K_H \times x_{CO_2} \quad (8)$$

where P is the reservoir pressure for measuring the CO_2 solubility, x_{CO_2} is the mole fraction of CO_2 at this pressure. The solubility is inversely related to the Henry coefficient. Thus, the solubility order is 1-oct > 3p > 1p > 2p > 3 > 1 > 2.

Henry coefficients at low temperatures were determined using the Arrhenius relationship. Fig. 9a shows the correlation of the Henry coefficient between simulation and experiment at 303 K for the np and n series ionic liquids. It was found that the solubility order remains the same except that 1p and 1 are higher than 3p and 3, respectively. Interestingly, it was found that the correlation of the Henry coefficient is similar to the density correlation in Fig. 3b, where n and np show two different types of correlations. The smaller slope of the np series indicates lower Henry coefficients than the n series, thus, the higher solubility. The simulated Henry's Law coefficients are approximately twice the experimental Henry's Law coefficients; however, the trends are in good agreement with the exception of 1-oct. In the simulation, 1-oct has the lowest K_H value (28.4 bar), but in experiments, 1p has the lowest K_H (23.4 bar) followed by 3p (27.2 bar) and finally 1-oct. The reason for this discrepancy is the combination of the effect of the heat of adsorption of CO_2 in the ionic liquid and the molar volume of the ionic liquid, which is difficult to rationalize since these two terms are not well correlated. However, the correlation in Fig. 9a clearly shows that 1-oct is the lowest in the simulation because the n series has a higher negative slope than np series.

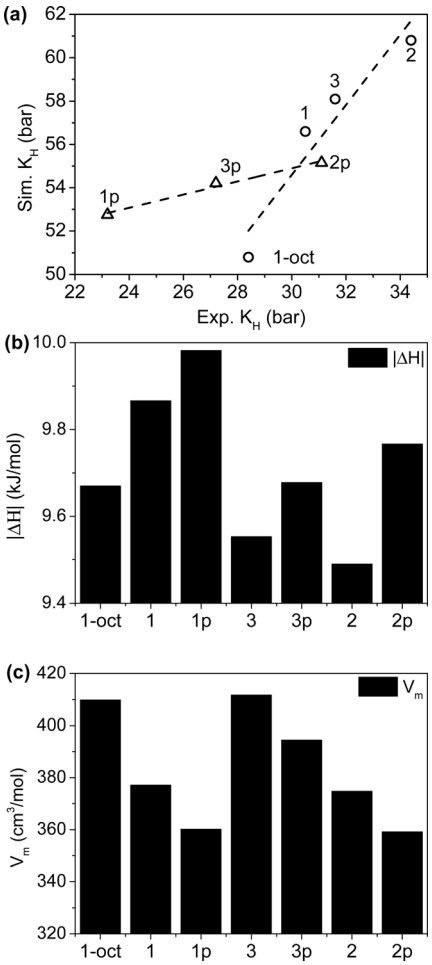

Fig. 9 (a) Correlation between experiment and simulation K_H at temperature 303 K, all data are listed in Table S1-6 (ESI†). (b) Simulated heat adsorption of CO_2 in ionic liquids, and (c) simulated molar volume of these ionic liquids, all data are listed in Table S1-7 (ESI†).

Fig. 9b and c show the CO_2 heat of adsorption in the ionic liquids, and the molar volume of these ionic liquids at 303 K. The CO_2 heat of adsorption shows the strength of CO_2 interacting with the ionic liquids: the higher the heat of adsorption, the higher the CO_2 solubility. The molar volume is another factor that influences CO_2 solubility. It is observed that the higher the molar volume, the more CO_2 is adsorbed. Fig. 9b shows that np type ionic liquids have higher absolute heats of adsorption than n type ionic liquids. Despite the fact that the molar volume of np is smaller than n, it has higher CO_2 solubility. For 1-oct and 1, 1 has a higher heat of adsorption than 1-oct; however, the lower molar volume of 1-oct contributes more resulting in higher solubility for 1-oct. For different functional groups, in the np series, the solubility order is 1p > 3p > 2p and is observed in both simulation and experiment. For the n series, the solubility order is 1-oct > 1 > 3 > 2 in both simulation and experiment.

To study the CO_2 interaction with ionic liquids in microscopic detail, CO_2 was mixed with all ionic liquids at 303 K and 5 bar. Numbers of CO_2 molecules based on eqn (8) were calculated. The densities after the CO_2 addition decreased less than 0.5%. Fig. 10a compares the cation–anion RDFs in ionic liquid 1 and a mixture of 1 and CO_2. The similarities between the RDFs suggest that CO_2 does not disturb the ionic liquid structure, which is due to the strong coulombic interactions between the cation and the anion, just as observed in mixtures of CO_2 and imidazolium-based ionic liquids.[13,14] In order to understand how CO_2 orients itself in the network the center of mass of CO_2–cation and center of mass of CO_2–anion RDFs in a mixture of 1 and CO_2 were calculated. Fig. 10b shows that CO_2 interacts more strongly with the anion than with the cation. In addition, the intensity of the CO_2–cation RDF approaches unity, which implies that the CO_2 molecules distribute randomly with respect to the cation. Fig. 10c shows how CO_2 interacts with parts of the anion, CO_2 interacts most strongly with the side CF_3 groups, then the central N atom, and the SO_2 group. Fig. 10d also shows how CO_2 interacts with parts of the cation. CO_2 interacts strongly with the methyl (R_3) side group. However, CO_2 does not form a structural RDF with the triazolium core nor the acidic proton at the HA-position on the ring, which may be because HA lies between the bulky R_1 and R_2 side groups, and the interaction of CO_2 with HA is sterically hindered. As a contrast, the CH_3 side group is most exposed, so CO_2 molecules can orient between R_3 and the anion to maximize their interaction with anions. The RDFs of CO_2 with other ionic liquids exhibit similar properties as ionic liquid 1, as shown in Fig. S4-1–S4-3 (ESI†).

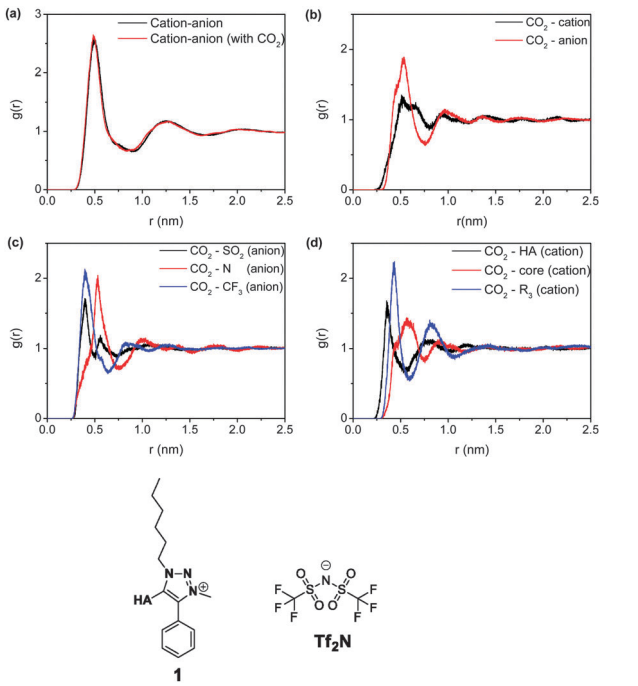

Fig. 10 (a) RDFs of cation–anion of ionic liquid 1 and ionic liquid 1 mixture with CO_2 at 303 K and 5 bar. (b) RDFs of CO_2–anion and CO_2–cation of ionic liquid 1 mixture with CO_2. (c) RDFs of CO_2 with CF_3, N and SO_2 of anion TF_2N. (d) RDFs of CO_2 with CH_3, HA, and core of cation 1.

5. Conclusions

In this work we have developed new force fields and validated our results with experimental data. We have used the methodology developed by Lopes[28,29] to build a force field for a class of ionic liquids. The important advantage of this approach is that the resulting force field is compatible with the OPLS[33] and the Amber force field.[32] This has an important practical advantage as one can use our force field to, for example, study the properties of these ionic liquids in a polymer matrix. For the polymer and the polymer–ionic liquid interactions the OPLS[33] or Amber force fields[32] can be used. As these force fields have tested for many systems one can expect a reasonable description of the system. This transferability was our main motivation to use the Lopes approach.[28,29]

This transferability clearly has its limitation. We observe that the densities of the ILs are systematically overestimated. If the densities are off by only 3%, we can expect much large deviations on those properties that rely on an accurate description of the density. Indeed, we see much larger deviation for our predictions of the CO_2 diffusion coefficient and the solubility. As the deviations in the densities are systematic, so are the deviations in the CO_2 diffusion coefficient and the solubility, we can ''correct'' for these deviations using a few experimental data points. As a consequence this model allows us to make reasonable predictions if we apply these corrections.

It would be interesting to see whether extensions of the present force field would allow us to improve the predictions. We feel that a key aspect is to improve the predictions of the densities. Possible directions would be to include polarization[45] or different methods for the charge distribution.[46]

Overall, the trends predicted by simulation agree with experimental data giving excellent insight into the effect of side groups and how they influence the self-diffusion coefficient and CO_2 solubility. The insights gained here due to the influence of side groups are important in the development of ionic liquid materials and can be used for quick screening of a diverse set of ionic liquids.

Acknowledgements

ML, KD, EA, RLT, HBN, and DRL gratefully acknowledge the financial support by the United States Department of Energy's Office of Fossil Energy under the National Energy Technology Laboratory Field Work Proposal Car Cap_FY131415. FY and JK are supported by the Assistant Secretary for Fossil Energy of the U.S. Department of Energy under Contract No. DE-AC02-05CH11231. MH and B.S. were supported as part of the Center for Gas Separations Relevant to Clean Energy Technologies, an Energy Frontier Research Center funded by the U.S. Department of Energy, Office of Science, Office of Basic Energy Sciences under Award Number DE-SC0001015. Berkeley Lab is supported by the Office of Science of the U.S. Department of Energy under Contract No. DE-AC02-05CH11231. This research used resources of the National Energy Research Scientific Computing Center, which is supported by the Office of Science of the U.S. Department of Energy under Contract No. DE-AC02-05CH11231. We thank Li-Chiang Lin for helping to prepare the figures. This project was funded by the Department of Energy, National Energy Technology Laboratory, an agency of the United States Government, through a support contract with URS Energy & Construction, Inc. Neither the United States Government nor any agency thereof, nor any of their employees, nor URS Energy & Construction, Inc., nor any of their employees, makes any warranty, expressed or implied, or assumes any legal liability or responsibility for the accuracy, completeness, or usefulness of any information, apparatus, product, or process disclosed, or represents that its use would not infringe privately owned rights. Reference herein to any specific commercial product, process, or service by trade name, trademark, manufacturer, or otherwise, does not necessarily constitute or imply its endorsement, recommendation, or favoring by the United States Government or any agency thereof. The views and opinions of authors expressed herein do not necessarily state or reflect those of the United States Government or any agency thereof.

Notes and references

1 J. Wilcox, *Carbon Capture*, Springer Verlag, 2012.
2 D. M. D'Alessandro, B. Smit and J. R. Long, *Angew. Chem., Int. Ed.*, 2010, **49**, 6058.
3 H. W. Perinline, D. R. Luebke, K. L. Jones, C. R. Myers, B. I. Morsi, Y. J. Heintz and J. B. Ilconich, *Fuel Process. Technol.*, 2008, **89**, 897.
4 X. P. Zhang, X. C. Zhang, H. F. Dong, Z. J. Zhao, S. J. Zhang and Y. Huang, *Energy Environ. Sci.*, 2012, **5**, 6668.
5 F. Karadas, M. Atilhan and S. Aparicio, *Energy Fuels*, 2010, **24**, 5817.
6 A. R. Katritzky, R. Jain, A. Lomaka, R. Petrukhin, M. Karelson, A. E. Visser and R. D. Rogers, *J. Chem. Inf. Comput. Sci.*, 2002, **42**, 225.
7 J. F. Brennecke and B. E. Gurkan, *J. Phys. Chem. Lett.*, 2010, **1**, 3459.
8 J. F. Brennecke and E. J. Maginn, *AIChE J.*, 2001, **47**, 2384.
9 E. D. Bates, R. D. Mayton, I. Ntai and J. H. Davis, *J. Am. Chem. Soc.*, 2002, **124**, 926.
10 J. H. Huang and T. Ruther, *Aust. J. Chem.*, 2009, **62**, 298.
11 B. Gurkan, B. F. Goodrich, E. M. Mindrup, L. E. Ficke, M. Massel, S. Seo, T. P. Senftle, H. Wu, M. F. Glaser, J. K. Shah, E. J. Maginn, J. F. Brennecke and W. F. Schneider, *J. Phys. Chem. Lett.*, 2010, **1**, 3494.
12 J. L. Anthony, J. L. Anderson, E. J. Maginn and J. F. Brennecke, *J. Phys. Chem. B*, 2005, **109**, 6366.
13 C. Cadena, J. L. Anthony, J. K. Shah, T. I. Morrow, J. F. Brennecke and E. J. Maginn, *J. Am. Chem. Soc.*, 2004, **126**, 5300.
14 X. H. Huang, C. J. Margulis, Y. H. Li and B. J. Berne, *J. Am. Chem. Soc.*, 2005, **127**, 17842.
15 D. Kerle, R. Ludwig, A. Geiger and D. Paschek, *J. Phys. Chem. B*, 2009, **113**, 12727.
16 J. K. Shah and E. J. Maginn, *J. Phys. Chem. B*, 2005, **109**, 10395.

17 E. J. Maginn, *J. Phys.: Condens. Matter*, 2009, **21**, 373101.
18 J. L. Anthony, E. J. Maginn and J. F. Brennecke, *J. Phys. Chem. B*, 2001, **105**, 10942.
19 C. P. Fredlake, J. M. Crosthwaite, D. G. Hert, S. N. V. K. Aki and J. F. Brennecke, *J. Chem. Eng. Data*, 2004, **49**, 954.
20 S. N. V. K. Aki, B. R. Mellein, E. M. Saurer and J. F. Brennecke, *J. Phys. Chem. B*, 2004, **108**, 20355.
21 H. B. Nulwala, C. N. Tang, B. W. Kail, K. Damodaran, P. Kaur, S. Wickramanayake, W. Shi and D. R. Luebke, *Green Chem.*, 2011, **13**, 3345.
22 E. W. Lemmon, M. L. Huber and M. O. McLinden, *NIST Standard Reference Database 23: Reference Fluid Thermodynamic and Transport Properties – REFPROP*, Gaithersburg, 2010.
23 E. W. Lemmon and R. Tillner-Roth, *Fluid Phase Equilib.*, 1999, **165**, 1.
24 R. M. Cotts, M. J. R. Hoch, T. Sun and J. T. Markert, *J. Magn. Reson. (1969)*, 1989, **83**, 252.
25 D. H. Wu, A. D. Chen and C. S. Johnson, *J. Magn. Reson., Ser. A*, 1995, **115**, 260.
26 J. E. Tanner, *J. Chem. Phys.*, 1970, **52**, 2523.
27 E. O. Stejskal and J. E. Tanner, *J. Chem. Phys.*, 1965, **42**, 288.
28 J. N. C. Lopes, J. Deschamps and A. A. H. Pádua, *J. Phys. Chem. B*, 2004, **108**, 2038.
29 J. N. C. Lopes and A. A. H. Pádua, *J. Phys. Chem. B*, 2004, **108**, 16893.
30 M. J. Frisch, G. W. Trucks, H. B. Schlegel, G. E. Scuseria, M. A. Robb, J. R. Cheeseman, J. A. Montgomery, T. Vreven, K. N. Kudin and J. C. Burant, *Gaussian 03 Revision C.02*, Gaussian, Inc., Pittsburgh PA, 2003.
31 C. M. Breneman and K. B. Wiberg, *J. Comput. Chem.*, 1990, **11**, 361.
32 W. D. Cornell, P. Cieplak, C. I. Bayly, I. R. Gould, K. M. Merz, D. M. Ferguson, D. C. Spellmeyer, T. Fox, J. W. Caldwell and P. A. Kollman, *J. Am. Chem. Soc.*, 1995, **117**, 5179.
33 W. L. Jorgensen, D. S. Maxwell and J. Tirado-Rives, *J. Am. Chem. Soc.*, 1996, **118**, 11225.
34 J. Wang, R. M. Wolf, J. W. Caldwell, P. A. Kollman and D. A. Case, *J. Comput. Chem.*, 2004, **25**, 1157.
35 B. Hess, C. Kutzner, D. van der Spoel and E. Lindahl, *J. Chem. Theory Comput.*, 2008, **4**, 435.
36 U. Essmann, L. Perera, M. L. Berkowitz, T. Darden, H. Lee and L. G. Pedersen, *J. Chem. Phys.*, 1995, **103**, 8577.
37 S. Nosé, *Mol. Phys.*, 1984, **52**, 255.
38 W. G. Hoover, *Phys. Rev. A*, 1985, **31**, 1695.
39 M. Parrinello and A. Rahman, *J. Appl. Phys.*, 1981, **52**, 7182.
40 Y. Wang and G. A. Voth, *J. Am. Chem. Soc.*, 2005, **127**, 12192.
41 E. J. Maginn, *Acc. Chem. Res.*, 2007, **40**, 1200.
42 J. G. Harris and K. H. Yung, *J. Phys. Chem.*, 1995, **99**, 12021.
43 B. Widom, *J. Chem. Phys.*, 1963, **39**, 2808.
44 D. Frenkel and B. Smit, *Understanding Molecular Simulation from Algorithms to Applications*, Academic Press, San Diego, CA, 2002.
45 O. Borodin, *J. Phys. Chem. B*, 2009, **113**, 11463.
46 M. Klähn, A. Seduraman and P. Wu, *J. Phys. Chem. B*, 2008, **112**, 10989.

